A Solid-State NMR, X-ray Diffraction, and Ab Initio Investigation into the Structures of Novel Tantalum Oxyfluoride Clusters

ARTICLE *in* CHEMISTRY OF MATERIALS · FEBRUARY 2008

Impact Factor: 8.35 · DOI: 10.1021/cm0717763

7 AUTHORS, INCLUDING:

Todd M Alam
Sandia National Laboratories
265 PUBLICATIONS **4,036** CITATIONS
SEE PROFILE

Steven G. Thoma
Thoma Technologies
50 PUBLICATIONS **540** CITATIONS
SEE PROFILE

Mark A Rodriguez
Sandia National Laboratories
278 PUBLICATIONS **4,094** CITATIONS
SEE PROFILE

Shaohui Zheng
University of Michigan
18 PUBLICATIONS **317** CITATIONS
SEE PROFILE

A Solid-State NMR, X-ray Diffraction, and Ab Initio Investigation into the Structures of Novel Tantalum Oxyfluoride Clusters

Todd M. Alam,*,† Jacalyn S. Clawson,†,‡ François Bonhomme,† Steven G. Thoma,† Mark A. Rodriguez,† Shaohui Zheng,§ and Jochen Autschbach§

Department of Electronic and Nanostructured Materials, Department of Geochemistry, Department of Materials Characterization, and Department of Fuels and Energy Transitions, Sandia National Laboratories, Albuquerque, New Mexico 87185, and Department of Chemistry, University at Buffalo, State University of New York, Buffalo, New York 14260-3000

Received July 5, 2007. Revised Manuscript Received December 12, 2007

A series of tantalum oxyfluoride materials containing the $[Ta_4F_{16}O_4]^{4-}$ and $[Ta_8F_{24}O_{12}]^{8-}$ anion clusters have been synthesized and characterized using X-ray diffraction (XRD) and solid-state nuclear magnetic resonance (SSNMR) spectroscopy. The structure of both tantalum oxyfluoride materials display octahedrally bonded tantalum atoms with bridging oxygen and terminal fluoride atoms. The $[Ta_4F_{16}O_4]^{4-}$ cluster is an eight-membered ring, whereas the $[Ta_8F_{24}O_{12}]^{8-}$ cluster forms a cagelike structure. Solid-state dynamics of these clusters were explored by monitoring the impact of temperature on the one-dimensional (1D) ^{19}F magic angle spinning (MAS) NMR, ^{13}C cross-polarization (CP) MAS NMR, and two-dimensional (2D) double quantum (DQ) ^{19}F MAS NMR spectra. The DQ ^{19}F NMR correlation experiments allowed the through space connectivity between the different resolved fluorine environments to be determined, thus aiding in the spectral assignment and structural refinement of these materials. Ab initio ^{19}F NMR chemical shift calculations were used to assist in the interpretation of the ^{19}F NMR spectra. The influence of scalar relativistic and Ta−F spin–orbit coupling on the ^{19}F NMR shielding calculation arising from bonding to tantalum atoms is also addressed.

Introduction

Tantalum oxide is used as a catalyst and promoter in various industrial organic syntheses.[1,2] For these applications controlled pore and open structure compounds are of great value, yet the relative insolubility of tantalum oxide negates many of the typical hydro- or solvothermal synthesis routes for open structure materials. Tantalum does however, readily form a variety of fluorine compounds.[3] Understanding the coordination chemistry of tantalum, along with the development of open structure tantalum fluoride compounds, may provide a means to create new, industrially relevant tantalum materials.

Tantalum oxyfluoride anionic clusters have been previously reported including the $[TaF_6]^-$ anion,[4] a series of $[TaF_7]^{2-}$ polyhedron anions,[5–7] the $[Ta(O_2)F_5]^{2-}$ and $[TaF_5O]^{2-}$ anions,[8,9] the linear $[Ta_2F_{10}O]^{2-}$ dimer,[10] and the adamantane-like cage $[Ta_4F_{12}O_6]^{4-}$ anion.[11] These systems demonstrate a progression in the complexity and size of the oxyfluoro-tantalum cluster. Most of these TaF clusters have been characterized using single-crystal X-ray structural determination. In this paper, two novel tantalum oxyfluoride clusters, $[Ta_4F_{16}O_4]^{4-}$ (TAF16) and $[Ta_8F_{24}O_{12}]^{8-}$ (TAF24), are described (see Figure 1). In these materials the inorganic TaF clusters are counter balanced by organic cations. Two compounds containing the TAF24 cluster are characterized, one sample containing the imidazole countercation (TAF24-IMI) and the other containing the *tris*(2-aminoethyl)amine countercation (TAF24-TREN). The third compound characterized is the TAF16 cluster with a pyridinium counterion (TAF16-PYR).

Because the properties of these compounds are closely related to their structure it is important to structurally characterize these materials as fully as possible. For example, the ferroelectric properties are sensitive to the degree of fluorine-oxygen substitution.[3] In this paper, we utilize X-ray diffraction (XRD) and multinuclear (^{19}F, ^{13}C, ^{1}H) solid-state nuclear magnetic resonance (SSNMR) spectroscopy to understand the solid-state structure and dynamics of these

* To whom correspondence should be addressed. Phone: (505) 844-1225. Fax: (505) 844-2974. E-mail:tmalam@sandia.gov.
† Sandia National Laboratories.
‡ Present address: GlaxoSmithKline Plc, King of Prussia, PA 19406.
§ University at Buffalo, State University of New York.

(1) Ushikubo, T. *Catal. Today* **2000**, *57*, 331.
(2) Lambert, J. B., Tantalum and Tantalum Compounds. In *Kirk−Othmer Encyclopedia of Chemical Technology*; John Wiley & Sons: New York, 2001.
(3) Agulyansky, A. *The Chemistry of Tantalum and Niobium Fluoride Compounds*, 1st ed.; Elsevier: New York, 2005; p 407.
(4) Edwards, A. J.; Jones, G. R. *J. Chem. Soc. A: Inorg., Phys., Theor.* **1970**, 1891.
(5) Saada, M. A.; Hémon-Ribaud, A.; Smiri, L. S.; Leblanc, M.; Maisonneuve, V. *J. Fluorine Chem.* **2005**, *126*, 1246.
(6) Torardi, C. C.; Brixner, L. H.; Blasse, G. *J. Solid State Chem.* **1987**, *67*, 21.
(7) Goreshnik, E.; Leblanc, M.; Maisonneuve, V. *J. Solid State Chem.* **2004**, *177*, 4023.
(8) Ruzic-Toros, Z.; Kojic-Prodic, B. *Acta Crystallogr., Sect. B* **1976**, *B32*, 1096.
(9) Furmanova, N. G.; Verin, I. A.; Zanin, I. E.; Zozulin, A. N.; Il'in, E. G. *Sov. Phys. Crystallography* **1991**, *36*, 204.
(10) Dewan, J. C.; Edwards, A. J.; Calves, J. Y.; Guerchais, J. E. *J. Chem. Soc., Dalton Trans.* **1977**, 978.
(11) Sala-Pala, J.; Guerchais, J. E.; Edwards, A. J. *Angew. Chem., Int. Ed.* **1982**, *21*, 870.

10.1021/cm0717763 CCC: $40.75
Published on Web 02/16/2008

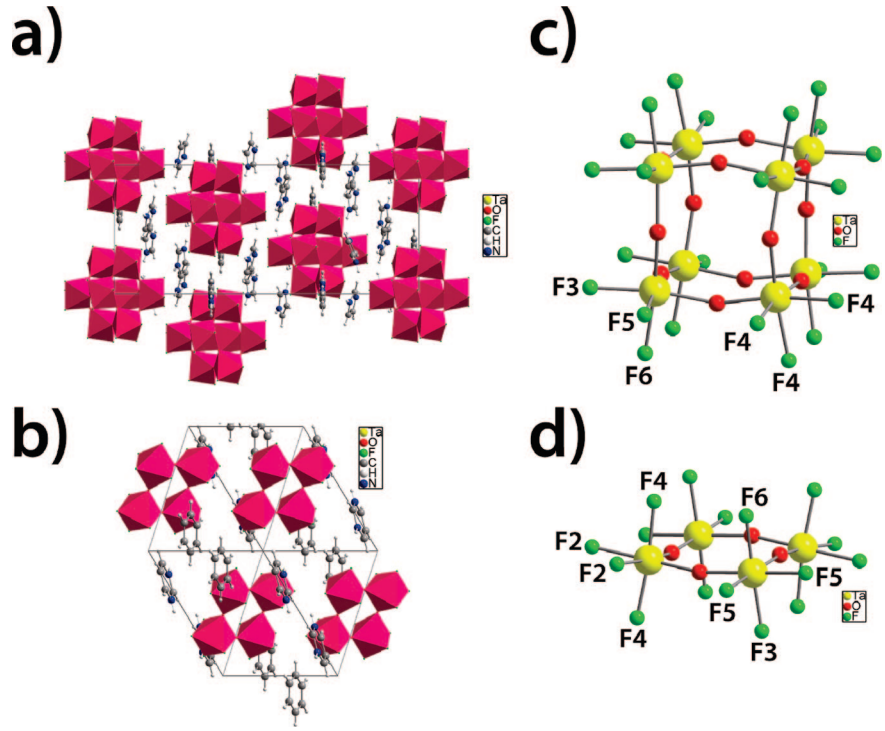

Figure 1. (a) TAF24-IMI unit cell along the *110* axis, and the (b) TAF16-PYR unit cell along the *111* axis. The colored Ta−O−F anion polyhedra making up the TAF clusters are shown with the organic counter cations in intercluster spaces. Structural representation of the Ta-O-F framework clusters for the (c) TAF24 and (d) TAF16 anions.

materials. XRD and SSNMR provide complementary structural information. XRD provides long-range ordering, whereas the SSNMR supplies information on the local environment of the probe nucleus. XRD is a valuable tool for obtaining the unit-cell parameters and atomic positions of the heavy atoms in well-ordered crystalline systems. However, in the case of the tantalum oxyfluorides, XRD has difficulty in distinguishing oxygen and fluorine ions, especially in powdered samples, since their ionic radii are similar. Furthermore, the organic counterions in these compounds are not well refined, suggesting significant disorder and/or multiplicities in the asymmetric unit. Because NMR probes the local environment, it is not susceptible to averaging due to disorder and provides structural details about the organic cations. SSNMR is also well-suited for studying the dynamics within the solid-state structure, which include the overall mobility of the molecules, motions of molecular groups, and chemical exchange.

High-speed ^{19}F magic angle spinning (MAS) NMR spectroscopy is a particularly attractive tool for the elucidation of structure because of its large chemical shift range (>1000 ppm).[12] However, ^{19}F SSNMR is technically demanding due in part to the large ^{19}F chemical shift anisotropy (CSA) and significant ^{19}F−^{19}F dipolar coupling, often requiring high-speed MAS (>30 kHz) to resolve the resonances. Additionally, specifically designed probes with low fluorine backgrounds must be available. Modern SSNMR systems are now commercially available that allow investigations of systems like the tantalum oxyfluoride clusters presented here. The interpretation of the ^{19}F MAS NMR spectra for Ta−F compounds is also difficult because of the small number of previously reported solid-state ^{19}F NMR studies. Therefore a good deal of this paper is devoted to assigning the solid state ^{19}F NMR results, and to understanding how the observed ^{19}F chemical shift is influenced by the TAF structure. We have employed two-dimensional (2D) double quantum (DQ) ^{19}F MAS NMR experiments, structure-shielding relationships from the solution-state along with ab initio density functional theory (DFT) NMR shielding calculations to address these issues.

(12) Harris, R. K.; Jackson, P. *Chem. Rev.* **1991**, *91*, 1427.

Experimental Section

Materials and Synthesis. All of the following materials were used as received: tantalum(V) fluoride, TaF_5 (99.8%, Aldrich), imidazole (99.5+ %, Aldrich), pyridine (99+%, Aldrich), and tris-2-amino ethyl amine, TREN (96%, Aldrich). Elemental analyses were carried out by Galbraith Laboratories (Knoxville, TN) using ICP-MS for Ta, combustion method for C, N and H and ion selective electrode for F.

TAF24-IMI, $[Ta_8O_{12}F_{24}]^{8-}\cdot 8(N_2C_3H_5)^+$. TaF_5 (1.38 g, 5 mmol) was dissolved at room temperature (RT) in 50 g of DI H_2O; imidazole (0.68 g, 10 mmol) was dissolved at RT in 4 g of DI H_2O. The two solutions were mixed and the resulting clear solution of pH 2.80 was left to evaporate at RT in an open beaker. In the course of 2 weeks, crops of transparent yellowish bipyramidal crystals up to 500 μm in size were recovered, washed with DI water and ethanol, and dried in air overnight at RT. The overall yield of the reaction was 73% (1.21 g of recovered product).

TAF24-TREN, $[Ta_8O_{12}F_{24}]^{8-}\cdot 2[(C_2H_4NH_3)_3NH]^{4+}\cdot 6\ H_2O$. TaF_5 (0.55 g, 2 mmol) was dissolved at RT in 2.5 g DI H_2O in a 23 mL Teflon-lined steel autoclave. TREN (0.12 g, 8.2 mmol) was added to the solution, which was stirred at RT for 15 min and then hydrothermally treated at 125 °C for 60 h. The resulting off-white crystalline powder was recovered by filtration; washed with DI

water, ethanol, and acetone; and left to dry in air overnight at RT. The yield was 40% (0.25 g of recovered product).

TAF16-PYR, $[Ta_4O_4F_{16}]^{4-}\cdot 4\,(NC_5H_6)^+$. TaF_5 (0.55 g, 2 mmol) was dissolved at RT in 2 g of DI H_2O in a 23 mL Teflon-lined steel autoclave. Pyridine (0.32 g, 4 mmol) was added to the solution, which was stirred at RT for 30 min and then hydrothermally treated at 170 °C for 24 h. The resulting white translucent crystals up to 500 μm in size were recovered by filtration; washed with DI H_2O, and ethanol; and dried in air at RT. A SEM of the resulting crystals is shown in Figure S1 in the Supporting Information. The overall yield was 45% (0.45 g of recovered product).

X-ray Diffraction (XRD). Single-crystal XRD data for TAF24-IMI and TAF16-PYR were collected with Mo Kα radiation (λ = 0.71073 Å) on a Bruker Smart CCD diffractometer at low temperature (173 and 168 K) and integrated with the Saint-Plus software. A RT (300 K) single-crystal data set was also obtained for TAF16-PYR. Empirical absorption corrections were carried out by the program SADABS. The structures were solved by direct methods (SIR97)[13] completed by difference Fourier synthesis, and refined by full matrix least-squares on F^2 (SHELXL97).[14] Hydrogen atoms were placed geometrically and refined using the riding atom model.[15] For TAF24-IMI one of the imidazole molecules in the unit cell was observed to be disordered at $x = 0$, $y = 0$, $z = 0.318$ (disordered about *c*-axis) with five other disordered imidazole dictated by symmetry. Similarly for TAF16-PYR a disordered pyridinium cation was observed at $x = 0.316$, $y = 0$, and $z = 0.869$, with three other pyridiniums dictated by symmetry. These disordered cations were modeled using PLATON/SQUEEZE.[16,17] Summaries of the crystallographic data for TAF24-IMI and TAF16-PYR are given in Table S1 and the accompanying crystallographic information files (CIF) in the Supporting Information.

The RT structure of TAF24-TREN was solved using ab initio methods from X-ray powder diffraction data obtained using a Bruker D8 Advance diffractometer in Bragg-Bretano geometry using Ni-filtered Cu Kα radiation. The powder pattern was indexed with high figures of merit (F(20) = 105, M(20) = 197) by the program TREOR90[18] with a primitive cubic cell of ca. 4700 Å^3. The extinction laws are uniquely consistent with the space-group $Pa\bar{3}$. A LeBail[19] fit carried out with the program FULLPROF2K[20] confirmed the metric of the unit cell and the adequacy of the space group and converged to $\chi^2 = 7.06$. The structure was solved using the direct-space reverse Monte Carlo approach as implemented in FOX.[21] Two independent $Ta(O/F)_6$ semirigid octahedra were input in the model and their orientations and positions were optimized by FOX. A satisfactory solution was obtained after approximately one million Monte Carlo steps, with the octahedra linked to each other forming octanuclear clusters similar to the one observed in TAF24-IMI. The site bonded to two Ta atoms was attributed to an oxygen atom and the positions of the Ta, O, and F atoms was refined by the Rietveld method constraining the bond distances to be similar to the corresponding ones observed in TAF24-IMI. This assumption of O linkages was confirmed by the ^{19}F MAS NMR studies presented in this paper (see F/O disorder discussion below). At this stage, a difference Fourier map revealed the position of the single independent TREN molecule, with its central nitrogen atom located on a 3-fold axis. During the refinement, the N−C and C−C bond distances were constrained to commonly observed values for TREN, but no angular restraints were used, the conformation of the molecule being free to vary. Toward the end of the present structural refinement, residual electron density attributable to a water molecule was clearly detected on a general position. Its inclusion in the model allowed the final agreement indices to drop from $\chi^2 = 12.8$ and $R_{Bragg} = 7.0\%$ to $\chi^2 = 7.9$ and $R_{Bragg} = 4.6\%$. The presence of crystallization water is further confirmed by the TGA data (see the Supporting Information). The summary of powder structural data for TAF24-TREN, including the values of the geometrical constraints and the measurement conditions are given in Table S2, along with the fractional atomic coordinates in Table S3 (Supporting Information).

Solid-State NMR (SSNMR). All SSNMR spectra were collected on a Bruker Avance 400 spectrometer, operating at 400.16 MHz for ^{1}H, 376.52 MHz for ^{19}F, and 100.63 MHz for ^{13}C. The ^{19}F NMR experiments used a 2.5 mm Bruker ^{1}H/^{19}F/X probe. Direct Bloch decay ^{19}F MAS NMR spectra were recorded without ^{1}H decoupling at spinning frequencies (ν_R) between 26 and 35 kHz. The addition of 80 kHz of TPPM ^{1}H decoupling had no visible effect on the ^{19}F MAS NMR spectra (Figure S2, Supporting Information), indicating that 30 kHz spinning is sufficient to effectively average residual ^{1}H,^{19}F dipolar couplings in the tantalum oxyfluoride materials. Spinning at 30 kHz is known to increase the sample temperature by ~30 °C. Thus the sample temperature was calibrated using the ^{207}Pb chemical shift variation of a secondary external $Pb(NO_3)_2$ standard.[22,23] The reported temperature values have been corrected based on this calibration. The ^{19}F MAS NMR spectra were externally reference to the secondary Teflon standard, $\delta = -122.0$ with respect to $CFCl_3$, $\delta = 0.0$. The ramped ^{1}H → ^{13}C cross-polarization (CP) MAS NMR spectra were recorded on a 4 mm Bruker ^{1}H/X MAS NMR probe with 62 kHz ^{1}H TPPM decoupling, a 3–6 kHz spinning speed, and a 2 ms contact time. The ^{13}C MAS NMR spectra were externally referenced to carbonyl resonance of the secondary standard glycine, $\delta = +176.0$ with respect to TMS, $\delta = 0.0$.

The 2D DQ ^{19}F MAS NMR correlation experiments used an offset compensated back-to-back (BABA) multiple pulse train sequence for excitation and reconversion of the multiple quantum coherence.[24] These 2D DQ MAS NMR experiments used 64 rotor-synchronized t_1 increments, a spinning rate of 30 kHz, a 2.5 μs $\pi/2$ pulses, and an excitation-reconversion length of $\tau_{exc} = 66.66$ μs. Phase sensitive detection in the F_1 dimension was obtained using the TPPI method.

Density Functional Theory Calculations. DFT calculations of the NMR parameters were performed with the 2005 version of the Amsterdam Density Functional (ADF)[25–27] package and with the Gaussian 03 (G03)[28] program. Geometries of the $[Ta_4F_{16}O_4]^{4-}$ (TAF16) and $[Ta_8F_{24}O_{12}]^{8-}$ (TAF24) anion clusters were obtained

(13) Altomare, A.; Burla, M. C.; Camalli, M.; Cascarano, G. L.; Giacovazzo, C.; Guagliardi, A.; Moliterni, A. G. G.; Polidori, G.; Spagna, R. *J. Appl. Crystallogr.* **1999**, *32*, 115.
(14) Sheldrick, G. M. *Programs for Crystal Structure Analysis Release 97–2*; Institüt für Anorganische der Universität: Göttingen, Germany, 1998.
(15) Busing, W. R.; Levy, H. A. *Acta Crystallogr.* **1964**, *17*, 142.
(16) Spek, A. L. *J. Appl. Crystallogr.* **2003**, *36*, 7.
(17) van der Sluis, P.; Spek, A. L. *Acta Crystallogr., Sect. A* **1990**, *46*, 194.
(18) Werner, P. E.; Eriksson, L.; Westdahl, M. J. *J. Appl. Crystallogr.* **1985**, *18*, 367.
(19) Le Bail, A.; Duroy, H.; Fourquet, J. *Mater. Res. Bull.* **1988**, *23*, 447.
(20) Rodriguez-Carvajal, J. A. FULLPROF: A Program for Rietveld refinement and pattern matching analysis, *Abstracts of the Satellite Meeting on Powder Diffraction of the XV Congress of the IUCr*, Toulouse, France, 1990; p 127.
(21) Favre-Nicolin, V.; Glusker, J. P.; Bock, C. W. *Inorg. Chem.* **1998**, *37*, 1853.
(22) Bielecki, A.; Burum, D. P. *J. Magn. Resonance, Ser. A* **1995**, *116*, 215.
(23) Takahashi, T.; Kawashima, H.; Sugisawa, H.; Baba, T. *Solid State Nucl. Magn. Reson.* **1999**, *15*, 119.
(24) Feike, M.; Demco, D. E.; Graf, R.; Gottwald, J.; Hafner, S.; Spiess, H. W. *J. Magn. Reson.* **1996**, *122*, 214.
(25) Guerra, C. F.; Visser, O.; Snijders, J. G.; te Velde, G.; Baerends, E. J., Parallelisation of the Amsterdam Density Functional Program. In *Methods and Techniques for Computational Chemistry*; Clementi, E., Corongiu, C. , Eds.; STEF: Cagliari, Italy, 1995; p 303.

from the respective diffraction structural data. Relativistic effects were accounted for in the shielding calculations using the zero-order regular approximation (ZORA)[29,30] density functional as implemented in ADF,[31] including both ZORA scalar (ZSC) and ZORA spin–orbit (ZSO) relativistic effects. Nonrelativistic (NR) computations were performed for comparison. The Becke Perdew (BP)[32,33] generalized gradient correction (GGA) density functional along with the Vosko−Wilk−Nusair (VWN)[34] local density approximation (LDA) were applied in the ADF calculations. The triple-ζ plus one polarization (TZP) Slater-type basis from the ADF basis set library[31] was employed. Since the ADF NMR program does not yet support hybrid functionals we have performed these calculations in G03 with the Becke's three-parameter hybrid functional (B3LYP).[35] The effective core potential Los Alamos with the double-ξ basis set (LANL2DZ) was used for the Ta atoms and should model the scalar relativistic effects. For F and O, the TZVP basis set was used, while for C and Cl the 6–311G(d) basis set was utilized.[36]

As a first-order approximation to crystal environment medium effects, a continuum model was applied. In the ADF calculations, the COnductorlike Screening MOdel (COSMO)[37–39]was applied, whereas in the G03 computations, the polarizable continuum model (PCM) was used.[40–44] The dielectric constant (DC) of pyridine was used in the PCM calculations. Calculated ^{19}F NMR chemical shifts are referenced to the computed shielding constants of $CFCl_3$ using $\delta = \sigma(CFCl_3) - \sigma$, where σ is the shielding constant for the fluorine of interest in parts per million. For the various computational models, we obtained the following fluorine shielding values for $CFCl_3$: $\sigma = +145$ ppm (G03/gas phase), $\sigma = +147$ ppm (G03/PCM), $\sigma = +145$ ppm, (ADF/COSMO), $\sigma = +118$ ppm (ADF/ZSC), $\sigma = +123$ ppm (ADF/ZSO), and $\delta = +120$ ppm (ADF/NR).

Table 1. Selected Structural Bond Distances and Angles for the TAF24 Clusters[a]

bond/angle	TAF24-IMI (173 K)	TAF24-TREN (298 K)
Ta1−F4	1.983(4) Å	1.942 Å
Ta2−F3	1.951(4) Å	1.894 Å
Ta2−F5	1.940(5) Å	1.859 Å
Ta2−F6	1.982(6) Å	1.915 Å
	Avg. = 1.96 Å	*Avg.* = 1.90 Å
Ta1−O2	1.879(5) Å	1.821 Å
Ta2−O1	1.891(4) Å	1.958 Å
Ta2−O2	1.921(5)Å	2.003 Å
	Avg. = 1.90 Å	*Avg.* = 1.94 Å
Ta1-Ta2	3.732(5) Å	3.674 Å
Ta2-Ta2	3.768(5) Å	3.736 Å
	Avg. = 3.75 Å	*Avg.* = 3.71 Å
Ta1−O2−Ta2	158.3(3)°	152.8°
Ta2−O2−Ta2	163.0(3)°	152.2°
	Avg. = 160.7°	*Avg.* = 152.5°

[a] See Figure 1c for atom numbering.

Results and Discussion

X-ray Diffraction. The XRD structures of these materials consist of octahedrally coordinated tantalum atoms with bridging oxygen atoms and terminal tantalum fluoride bonds surrounded by organic cations. The bond valence sums (BVS) for the isolated octanuclear $[Ta_8F_{24}O_{12}]^{8-}$ cluster in TAF24-IMI (Table S4, Supporting Information) or the tetranuclear $[Ta_4O_4F_{16}]^{4-}$ cluster in TAF16-PYR (Table S5, Supporting Information) shows that the fluorine atoms are under bonded, whereas the oxygen sites satisfy the valence with two O−Ta bonds. The under-bonded F show weak hydrogen bonding to the protons of the organic cations (and H_2O, in the case of TAF24-TREN). Although the O and F atoms are difficult to distinguish by X-ray diffraction because of the similarity of their scattering power, the Ta/F ratios determined from the chemical analyses and the ^{19}F MAS NMR results (see O/F disorder discussion) are consistent with O atoms occupying the bridging site between Ta atoms in the TAF clusters. Most of the previously described condensed transition metal oxo-fluoride phases exhibit a partially disordered oxygen−fluorine distribution, which does not appear to be the case for the TAF compounds presented here. The unit cell structures for the TAF24-IMI and TAF16-PYR materials are shown in panels a and b in Figure 1, respectively. Select bond distances and angles for the $[Ta_8F_{24}O_{12}]^{8-}$ (TAF24) clusters are given in Table 1, and in Table 2 for the $[Ta_4F_{16}O_4]^{4-}$ (TAF16) cluster. The observed bond distances and angles are consistent with the previously reported structures of the $[Ta_2F_{10}O]^{2-}$ dimer and the $[Ta_4F_{12}O_6]^{4-}$ cage cluster.[10,11]

(26) te Velde, G.; Bickelhaupt, F. M.; Baerends, E. J.; Gisbergen, S. J. A. v.; Guerra, C. F.; Snijders, J. G.; Ziegler, T. *J. Comput. Chem.* **2001**, *22*, 931.

(27) Baerends, E. J.; Autschbach, J.; Berces, A.; Bo, C.; Boerrigter, P. M.; Cavallo, L.; Chong, D. P.; Deng, L.; Dickson, R. M.; Ellis, D. E.; Fan, L.; Fischer, T. H.; Guerra, C. F.; van Gisbergen, S. J. A.; Groeneveld, J. A.; Gritsenko, O. V.; Gruning, M.; Harris, F. E.; van den Hoek, P.; Jacobsen, H.; van Kessel, G.; Kootstra, F.; van Lenthe, E.; Osinga, V. P.; Patchkovskii, S.; Philipsen, P. H. T.; Post, D.; Pye, C. C.; Ravenek, W.; Ros, P.; Schipper, P. R. T.; Schreckenbach, G.; Snijders, J. G.; Sola, M.; Swart, M.; Swerhone, D.; te Velde, G.; Vernooijs, P.; Versluis, L.; Visser, O.; van Wezenbeek, E.; Wiesenekker, G.; Wolff, S. K.; Woo, T. K.; Ziegler, T. *Amsterdam Density Functional Program (ADF)*; Vrije Universiteit Amsterdam: Amsterdam, 2005.

(28) Frisch, M J. ; Trucks, G. W.; Schlegel, H. B.; Scuseria, G. E.; Robb, M. A.; Cheeseman, J. R. J. A. Montgomery, J.; Vreven, T.; Kudin, K. N.; Burant, J. C.; Millam, J. M.; Iyengar, S. S.; Tomasi, J.; Barone, V.; Mennucci, B.; Cossi, M.; Scalmani, G.; Rega, N.; Petersson, G. A.; Nakatsuji, H.; Hada, M.; Ehara, M.; Toyota, K.; Fukuda, R.; Hasegawa, J.; Ishida, M.; Nakajima, T.; Honda, Y.; Kitao, O.; Nakai, H.; Klene, M.; Li, X.; Knox, J. E.; Hratchian, H. P.; Cross, J. B.; Bakken, V.; Adamo, C.; Jaramillo, J.; Gomperts, R.; Stratmann, R. E.; Yazyev, O.; Austin, A. J.; Cammi, R.; Pomelli, C.; Ochterski, J. W.; Ayala, P. Y.; Morokuma, K.; Voth, G. A.; Salvador, P.; Dannenberg, J. J.; Zakrzewski, V. G.; Dapprich, S.; Daniels, A. D.; Strain, M. C.; Farkas, O.; Malick, D. K.; Rabuck, A. D.; Raghavachari, K.; Foresman, J. B.; Ortiz, J. V.; Cui, Q.; Baboul, A. G.; Clifford, S.; Cioslowski, J.; Stefanov, B. B.; Liu, G.; Liashenko, A.; Piskorz, P.; Komaromi, I.; Martin, R. L.; Fox, D. J.; Keith, T.; Al-Laham, M. A.; Peng, C. Y.; Nanayakkara, A.; Challacombe, M.; Gill, P. M. W.; Johnson, B.; Chen, W.; Wong, M. W.; Gonzalez, C.; Pople, J. A. *Gaussian 03, Rev. C.02*, Gaussian Inc.: Pittsburg, PA, 2003.

(29) Dyall, K.; van Lenthe, E. *J. Chem. Phys.* **1999**, *111*, 1366.

(30) van Lenthe, E.; Baerends, E. J.; Snijders, J. G. *J. Chem. Phys.* **1993**, *99*, 4597.

(31) Wolff, S. K.; Ziegler, T.; van Lenthe, E.; Baerends, E. J. *J. Chem. Phys.* **1999**, *110*, 7689.

(32) Becke, A. D. *Phys. Rev. A* **1988**, *38*, 3098.

(33) Perdew, J. P. *Phys. Rev. B* **1986**, *33*, 8822.

(34) Vosko, S. H.; Wilk, L.; Nusair, M. *Can. J. Phys.* **1980**, *58*, 1200.

(35) Becke, A. D. *J. Chem. Phys.* **1993**, *98*, 5648.

(36) *Extensible Computational Chemistry Environment Basis Set Database*, Version 02/02/06; Pacific Northwest Laboratory: Richland, Washington, 2002.

(37) Klamt, A. *J. Phys. Chem.* **1995**, *99*, 2224.

(38) Klamt, A.; Jones, V. *J. Chem. Phys.* **1996**, *105*, 9972.

(39) Klamt, A.; Schuurmann, G. *J. Chem. Soc., Perkin Trans. 2* **1993**, 799.

(40) Miertus, S.; Scrocco, E.; Tomasi, J. *Chem. Phys.* **1981**, *55*, 117.

(41) Miertus, S.; Tomasi, J. *Chem. Phys.* **1982**, *65*, 239.

(42) Cossi, M.; Barone, V.; Cammi, R.; Tomasi, J. *Chem. Phys. Lett.* **1996**, 255.

(43) Silla, E.; Tunon, I.; Pascual-Ahuir, J. L. *J. Comput. Chem.* **1994**, 15.

(44) Tomasi, J.; Persico, M. *Chem. Rev.* **1994**, *94*, 2027.

Table 2. Selected Structural Bond Distances and Angles for TAF16-PYR (168 K)[a]

bond/angle	TAF16-PYR
Ta1−F3	1.885(15) Å
Ta1−F5	1.955(10) Å
Ta1−F6	1.879(13) Å
Ta2−F2	1.917(8) Å
Ta2−F4	1.898(8) Å
	Avg. = 1.91 Å
Ta1−O1	1.902(9) Å
Ta2-O2	1.859(46) Å
	Avg. = 1.88 Å
Ta1−Ta2	3.773(2) Å
Ta1−O1−Ta2	165.9(5)°
Ta1−O2−Ta2	144.4(5)°

[a] See Figure 1d for atom numbering.

TAF24 has a cage structure containing two unique tantalum sites, one with three equivalent fluorine sites [Ta1−$F4_3$] and another tantalum with three unique fluorine sites [Ta2−F3, −F5, −F6] (see Figure 1c). The TAF16 cluster is composed of an eight-membered ring containing two unique tantalum sites. The two axial fluorine F4 sites are crystallographically equivalent as well as the two equatorial fluorine F2 sites bonded to Ta1, whereas the axial fluorine sites F3 and F6 are unique on the Ta2 site (See Figure 1d). The thermal ellipsoids for the F atoms in the low-temperature (168 K) TAF16-PYR structure demonstrate significant elongation along one direction resulting in "egg-like" shaped ellipsoids. In the 300 K TAF16-PYR structure these thermal ellipsoids elongate in two dimensions resulting in thermal displacements that appear to have a more "pancake-like" symmetry. Neither of these F thermal ellipsoids is severe enough as to be of concern for the validity of the refinement. However, the data reveal that the directionality of the thermal motion is more pronounced in the low temperature structure. For the low temperature TAF16-PYR structure the O(1) and O(2) sites show a displacement disorder modeled by fractional occupancy of 0.84 and 0.16, respectively. In the RT structure the oxygen environments do not show disorder, which is also consistent with a well behaved Ta−O ring. All these observations indicate a tilting disorder of the TaO_2F_4 octahedra within the low-temperature structure, which could perhaps precede a phase transition.

Solid-State ^{19}F MAS NMR. The ^{19}F MAS NMR spectra of the TAF16 and TAF24 compounds collected at 327 K are shown in Figure 2 and the corresponding chemical shifts are listed in Table 3. TAF16-PYR has six slightly overlapping fluorine resonances at 327 K, whereas four fluorine resonances were observed in TAF24 spectra. All of these ^{19}F NMR resonances show multiple spinning sidebands (ssb) even at spinning speeds >30 kHz. The relative integrated intensities (including ssb) of the spectra are consistent with the fluorine ratios predicted by XRD. Unlike the other ^{19}F NMR resonances the $\delta = -197.3$ peak in TAF16-PYR has no associated ssb, contributes only 3.4% to the total ^{19}F spectral area, and shows no DQ correlations to any of the other ^{19}F resonances. Given the difference in the chemical shift tensor and small relative concentration, this resonance is likely due to an unknown impurity. The ^{19}F MAS NMR spectra of the TAF24 compounds do not show any of this impurity.

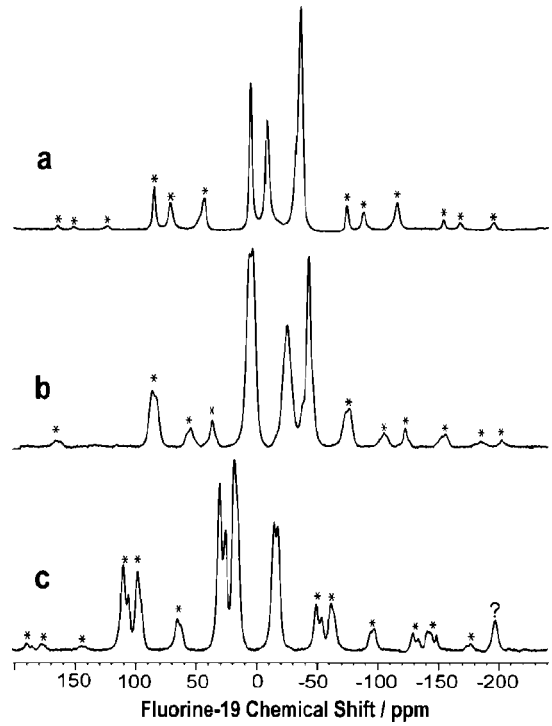

Figure 2. 1D ^{19}F MAS NMR spectra of (a) TAF24-IMI, (b) TAF24-TREN, and (c) TAF16-PYR collected at a sample temperature of 327 K and a spinning rate of 30 kHz. Spinning sidebands are marked with asterisks (*).

The ^{19}F MAS NMR spectra show large spinning sideband manifolds. In both clusters, the nearest fluorine neighbors are ~2.5 Å away, corresponding to a ^{19}F-^{19}F homonuclear dipolar coupling of 6.9 kHz for an isolated spin system. Under fast MAS, the ^{19}F−^{19}F homonuclear dipolar coupling (and ^{1}H−^{19}F heteronuclear dipolar coupling to the organic cations) is expected to be significantly reduced or removed such that the breadth of the spinning sideband patterns results from the large ^{19}F CSA. The small number of spinning sidebands (4) collected at 30 kHz leads to a large error in the measured principal values of the chemical shift tensor; therefore, the principal tensor values are not presented here and will be fully characterized in a future study.

The solid-state ^{19}F NMR chemical shifts are consistent with the wide range of chemical shifts previously reported for tantalum oxyfluoride compounds formed by the hydrolysis of tantalum pentafluoride, TaF_5. For example, the solution ^{19}F NMR chemical shift of the cubic $[Ta_4O_6F_{12}]^{2-}$ cage is observed at −27 ppm (in acetonitrile), the $[Ta_2O_2F_8]^{2-}$ ring cluster (in acetonitrile) shows two ^{19}F environments at $\delta = +23$ and −13 ppm,[45] the adamantane-like $[Ta_4F_{12}O_6]^{4-}$ cluster (in $CDCl_3$) shows a single resonance at $\delta = -28.5$,[11] the $[Ta_2F_{10}O]^{2-}$ dimer reveals resonances at $\delta = +32$ (equatorial) and $\delta = +13$ (axial), the $[Ta_2F_{11}]^{2-}$ dimer at $\delta = +72$ (equatorial) and $\delta = 115$ (axial), whereas the $[TaF_5O]^{2-}$ anion has been reported to have ^{19}F chemical shifts at approximately −10 and –95 ppm.[9] Given this wide range of ^{19}F chemical shifts reported previously in literature (−95 to +115 ppm), the assignment of the different ^{19}F

(45) Il'in, E. G.; Zozulin, A. N.; Buslaev, Y. A. *Dok. Phys. Chem.* **2002**, *384*, 109.

Table 3. Experimental ^{19}F NMR Chemical Shifts of Tantalum Oxyfluoride Clusters

compd	assignment	δ ^{19}F (ppm)[a] 327 K	fwhm[b] (Hz)	assignment	δ ^{19}F (ppm)[a] 253 K	fwhm[b] (Hz)
TAF24-IMI	F5	+6.3	900	F5	+10.4	960
	F3	−7.5	1320	F3	−8.3	1720
					−30.4[c]	1200
	F4	−31.8	1530	F4	−33.4[c]	1200
					−35.7[c]	1200
	F6	−35.2	1330	F6	−39.3	1160
TAF24-TREN	F5	+6.2	1750	F5	+7.1	1890
	F3	+2.4	1500	F3	+1.7	1680
	F4	−22.8[c]	1440	F4	−22.9[c]	1580
		−26.5[c]	2210		−26.6[c]	2790
	F6	−43.6	1350	F6	−44.6	1460
	F4	+30.1	1420	F4	+36.2	1320
TAF16-PYR				F4′	+20.4	1280
	F3	+25.4	1150	F3	+31.8	1320
				F3′	+24.8	1320
	F6	+18.0	1420	F6	+16.5	1320
				F6′	+8.6	1360
	F2	+18.0	1420	F2	+24.8	1320
	F2′	+14.8	1350	F2′	+11.4	1370
	F5	−14.2	1590	F5	−13.7	1430
	F5′		1440	F5′	−19.0	1430
				F5″	−24.2	1430

[a] Referenced to the secondary standard Teflon (δ = −122) with respect to $CFCl_3$ (δ = 0.0). [b] fwhm = Full width at half-maximum line width. [c] Broad unresolved resonance, arbitrarily deconvoluted using fixed fwhm.

resonances observed in the TAF16 and TAF24 materials is not trivial and will be detailed in the following sections.

Solid-State ^{13}C CP MAS NMR. The ^{13}C CP MAS NMR spectra and assignment of the three TAF compounds are shown in Figure 3 with the chemical shifts summarized in Table S6 (Supporting Information). The chemical shifts of TREN and the pyridinium cations are consistent with values reported in solution and were assigned subsequently.[46] Based on the ^{13}C SSNMR there was no evidence of exchange, disorder or multiple organic molecules in the asymmetric unit of the TA24-TREN and the TAF16-PYR materials. The ^{13}C SSNMR spectrum of the TAF24-IMI sample (Figure 3a) has four overlapping resonances at δ = +136.2, +135.2, +120.3, and +119.2 in an approximately 1:1:1:3 ratio. It should be noted that the C4/C5 resonances are overlapped such that the 1:3 ratio describes the spectral deconvolution, and not necessarily the ratio of the individual sites. Residual dipolar coupling between the ^{13}C and the neighboring ^{14}N (I = 1) nuclei can split the ^{13}C resonances into 2:1 doublets. However, at the current magnetic field strength of 9.4 T the effect of the coupling should be minimal and is not likely the source of the peak splitting. Imidazole also has two tautomeric structures, as shown in the Figure 3a (left inset). In solution, the NH proton of imidazole exchanges rapidly, making the C4 and C5 sites magnetically equivalent. For pure imidazole in the solid state, this exchange does not occur and the C4 and C5 sites are magnetically unique and resonate at two distinct shifts, δ = +126.8 and +115.5, respectively.[47] In the TAF24-IMI material, the protonated imidazole cation is expected, such that both nitrogens are protonated preventing this type of tautomeric exchange. The +136.2 and +135.2 ppm ^{13}C NMR resonances of *C*2, and the overlapping C4/C5 at +120.3 and +119.2 resonances observed in TAF24-IMI result from either two independent imidazole molecules in the asymmetric unit of the TAF24-IMI crystal,

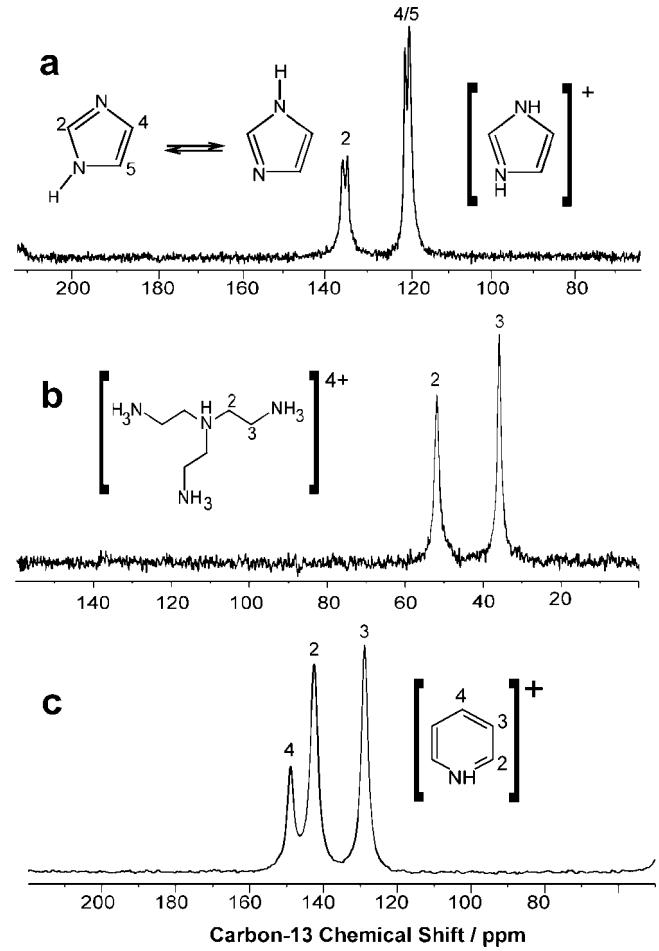

Figure 3. 1D ^{13}C CP MAS NMR spectra of (a) TAF24-IMI, (b) TAF24-TREN, and (c) TAF16-PYR at 295 K.

or an inequivalencies of the C2 and C4/C5 carbons due to differences in the adjacent NH hydrogen bonding environments.

Variable-Temperature (VT) Solid-State MAS NMR. To address the role of disorder and molecular motion on the observed NMR spectra a series of variable-temperature

(46) Pouchert, C. J.; Behnke, J., *The Aldrich Library of ^{13}C and ^{1}H FT NMR Spectra*, 1st ed.; Aldrich: St. Louis, MO, 1993.
(47) Thorpe, M. C.; Coburn, W. C., Jr *J. Magn. Reson.* **1973**, *12*, 225.

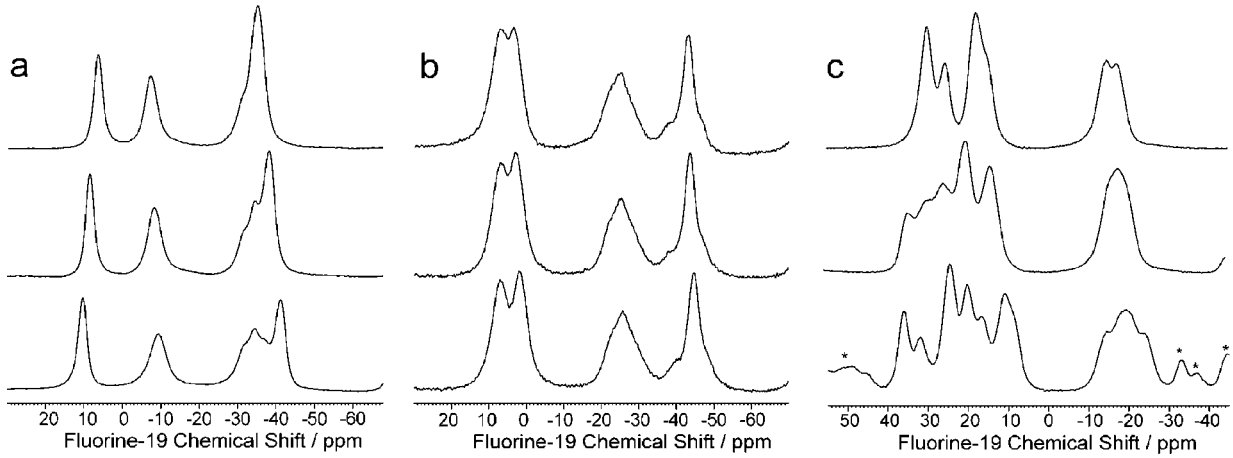

Figure 4. Isotropic region of the ^{19}F MAS NMR spectra as a function of temperature for (a) TAF24-IMI, (b) TAF24-TREN, and (c) TAF16-PYR collected at a sample temperature of 327 K (top), 283 K (middle), and 253 K (bottom). Spinning sidebands are denoted with asterisks (*).

studies were performed. Figure 4 shows the impact of reducing the temperature on the isotropic chemical shift region of the ^{19}F NMR spectra of the TAF16 and TAF24 materials. The ^{19}F NMR resonances at 327 and 253 K are summarized in Table 3. The ^{19}F NMR spectra of the TAF24 materials show only minor temperature variations. The largest change observed for the TAF24-IMI cluster were the two overlapping resonances between $\delta = -32$ and -35 (327 K) becoming more resolved at lower temperatures. The impact of temperature changes on the TAF16-PYR material is more dramatic, with the observation of multiple new resolved resonances at lower temperatures (Figure 4c). The spectral changes were all reversible, indicating that decomposition or irreversible phase changes did not occur upon heating/cooling. These VT results make sense considering the mobility associated with the ring (TAF16) compared to the more rigid (TAF24) cage structures.

This splitting of resonances in TAF16-PYR with decreasing temperature may result from slowing molecular motions such that the averaging of different ^{19}F environments is not occurring, and corresponds to exchange rates less than the frequency difference between the different ^{19}F environments. For example, the $\delta = +30.1$ ^{19}F NMR resonance of TAF16-PYR at 327 K splits into two resonances at $\delta = +36.2$ and $+20.4$ when the sample was cooled to 253 K (these assignments are based on the 2D DQ MAS NMR results discussed below), corresponding to a $\Delta\delta = 15.8$ or $\Delta\nu \sim 6000$ Hz. Therefore, a dynamic process on the order of 6000 Hz must be occurring at 327 K to average the two ^{19}F sites environments. The dynamic process could be an intramolecular rotation around the Ta atoms, or a bending or flipping of the ring, or a change in the relative orientation of the organic cation. The disorder observed in the ring oxygen in the low temperature X-ray structure of TAF16 (see discussion above) is consistent with a ring type motion. Nonetheless, the chemical nature and connectivity of the TAF16 cluster is maintained.

The VT ^{13}C CPMAS NMR spectra of TAF16-PYR were obtained to evaluate the disorder and/or dynamics of the organic counterion and its possible influence on the ^{19}F SSNMR spectra (See Figures S3 and S4, Supporting Information). On the basis of ab initio cluster calculations, small changes in the countercation orientation with respect to the TAF cluster can produce splittings in the predicted ^{19}F chemical shifts. However, experimentally, no changes were observed in the VT ^{13}C NMR spectra, arguing against large changes of the organic cation/cluster interaction. The differences in the time scales between the ^{13}C and ^{19}F SSNMR spectra should be noted. Motions on the order of $\sim$6000 Hz in the ^{19}F NMR spectra would correspond to a large $\Delta\delta(^{13}\text{C})$ of $\sim$60 ppm in the ^{13}C isotropic resonance. The changes in the ^{13}C NMR chemical shift of different organic structures are typically less than 10 ppm (1000 Hz). Since the time scale of the ^{13}C isotropic chemical shift is less than the 6000 Hz observed in the ^{19}F spectra, only the average chemical shift would be expected. On the other hand the spinning sidebands arising from the ^{13}C CSA range between $\sim$11 and 14.5 kHz and show no variation in breadth or intensity during the VT experiments (Figure S4). These VT results demonstrate that the dynamical process that is observed in the ^{19}F MAS NMR spectra (Figure 4) is occurring within the TaF cluster, and is not a result of dynamics within the surrounding organic cations.

It has also been suggested that the splitting of the ^{19}F MAS NMR resonances at lower temperatures may result from residual dipolar coupling between the quadrupolar ^{181}Ta nucleus ($I = 7/2$, 99.98% relative abundance) and ^{19}F. Variable temperature ^{19}F MAS NMR experiments at a higher magnetic field (Figure S5, Supporting Information) demonstrate that the observed ^{19}F resonance line shapes and splitting were invariant with increased magnetic field strength. As a first approximation, the dipolar interaction with a quadrupolar nuclei predicts the ^{19}F line splitting to scale proportionally with the residual dipolar coupling (R_{eff}) and the quadrupolar coupling of ^{181}Ta (C_{Q}), but scale inversely with the Larmor frequency of the quadrupolar nuclei (υ_{I}) as $\sim(3C_{\text{Q}}R_{\text{eff}}/20\upsilon_{\text{I}})$. Increasing the field strength by a factor of 1.5 should have reduced the ^{19}F line splitting, but this effect was not observed. It is noted that the high-field approximation holds for situations where $\upsilon_{\text{I}} \gg C_{\text{Q}}$, such that analysis for larger C_{Q} values require complete diagonalization of the interaction Hamiltonian.[48,49] The C_{Q} for TaF materials is not

(48) Heise, H.; Köhler, F. H.; Brouwer, E. B.; Harris, R. K.; Steuernagel, S. *Magn. Reson. Chem.* **1999**, *37*, 573.

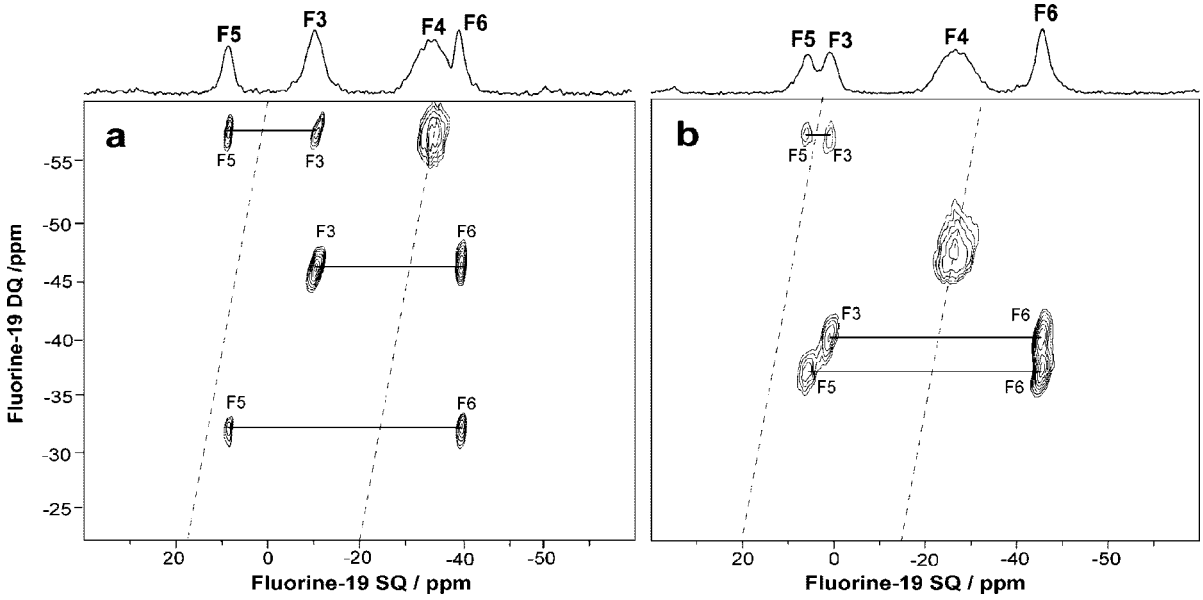

Figure 5. 2D DQ ^{19}F MAS NMR correlation spectra of (a) TAF24-IMI and (b) TAF24-TREN collected at a sample temperature of 253 K, and $\nu_R = 30$ kHz using a 66.6 μs excitation/reconversion BABA sequence. The different correlations are marked, with the single quantum projections shown on top.

know, but in TaO_3 compounds has been estimated as high as 250 GHz,[50] clearly outside the high-field approximation. Regardless of the C_Q magnitude, some variation of the line shape and splitting with changes in magnetic field strength is expected if a residual dipolar coupling between Ta and F were present. In addition, if this type of Ta-F dipolar coupling were significant we would expect it to be observable in all of the materials investigated, not simply the TAF16-PYR cluster. Although residual dipolar couplings to quadrupolar nuclei have been documented in a range of different materials,[48,51,52] we do not feel that for the TAF materials reported here the residual dipolar coupling between ^{19}F and ^{181}Ta is observed. Perhaps a fast T_1 relaxation of the quadrupolar ^{181}Ta nucleus has resulted in a self-decoupling from the ^{19}F nucleus. In conclusion, we argue that the ^{19}F NMR spectral variations observed as a function of temperature do not arise from coupling to the Ta, but instead arise from the ring motions leading to disorder of the bridging oxygen.

2D Double Quantum (DQ) ^{19}F MAS NMR. The 2D ^{19}F DQ MAS NMR experiments are based on through-space ^{19}F−^{19}F dipolar coupling (directly related to the F−F distances) and can be used to help assign the ^{19}F NMR spectra. The 2D DQ MAS NMR spectra for TAF24-IMI and TAF24-TREN are shown in Figure 5, whereas the 2D DQ MAS NMR spectra for TAF16-PYR at two different temperatures are shown in Figure 6 The DQ NMR experiment has an advantage over other dipolar correlation experiments in that diagonal autocorrelation peaks are only produced if ^{19}F environments with identical chemical shifts are dipolar coupled. On the basis of the experimental conditions of the BABA DQ MAS NMR experiment, dipolar couplings strengths >5 kHz (^{19}F−^{19}F distances less than ~3 Å) are expected to produce observable peak intensity in the 2D correlation experiment. The significant intra and intermolecular ^{19}F−^{19}F distances measured by XRD are summarized in Table 4. In the DQ MAS NMR spectra, the autocorrelation condition (through space connection of fluorine with the same chemical shift) is denoted by the diagonal dashed lines. For all the DQ spectra, the F_1 dimension has been folded due to the limited spectral width in the indirect dimension governed by the spinning speed used; nonetheless, the correlations can readily be identified.

For TAF24-IMI at 253 K, the 2D DQ ^{19}F MAS NMR spectrum (Figure 5a) shows several distinct strong cross-peak correlations between $\delta = +10.4/-8.3$, $+10.4/-39.3$, and $-8.3/-39.3$. The broad resonance at $\delta = -31.8$ shows a strong autocorrelation peak and no cross-correlation peaks to other ^{19}F environments. The unique dipolar coupling pattern of the DQ NMR demonstrate that the $\delta = -31.8$ resonance arises from multiple ^{19}F nuclei with similar chemical shifts that are dipolar coupled only to each other. This dipolar connectivity information is not available in the 1D spectrum. The lack of autocorrelation peaks for the other ^{19}F resonances reveal that each of these represent a single ^{19}F nuclei that is dipolar coupled to other distinct ^{19}F chemical shift environments. Similar results were observed in the TAF24-TREN DQ ^{19}F MAS NMR spectrum (Figure 5b), where strong correlation peaks were observed between $\delta = +7.1/-44.6$, $+1.7/-44.6$, a weak correlation between $\delta = +7.1/+1.7$ and an autocorrelation peak for the broad unresolved $\delta = -22.8$ resonance. These DQ correlations and corresponding dipolar connectivities are consistent with the fluorine sites observed in the XRD structure. The −31.8 (TAF24-IMI) and −22.8 ppm (TAF24-TREN) ^{19}F NMR resonances can be assigned to the three F4 sites bound to Ta(1), while the three resonances showing the cross-peaks to each other arise from the three distinct fluorine sites on

(49) Wi, S.; Frydman, V.; Frydman, L. *J. Chem. Phys.* **2001**, *114*, 8511.
(50) Rod, S.; Borsa, F.; van der Klink, J. J. *Phys. Rev. B* **1988**, *38*, 2267.
(51) Tang, J. A.; Ellis, B. D.; Warren, T. H.; Hanna, J. V.; Macdonald, C. L. B.; Schurko, R. W. *J. Am. Chem. Soc.* **2007**, *129*, 13049.
(52) Sastry, D. L.; Naito, A.; McDowell, C. A. *Chem. Phys. Lett.* **1988**, *146*, 422.

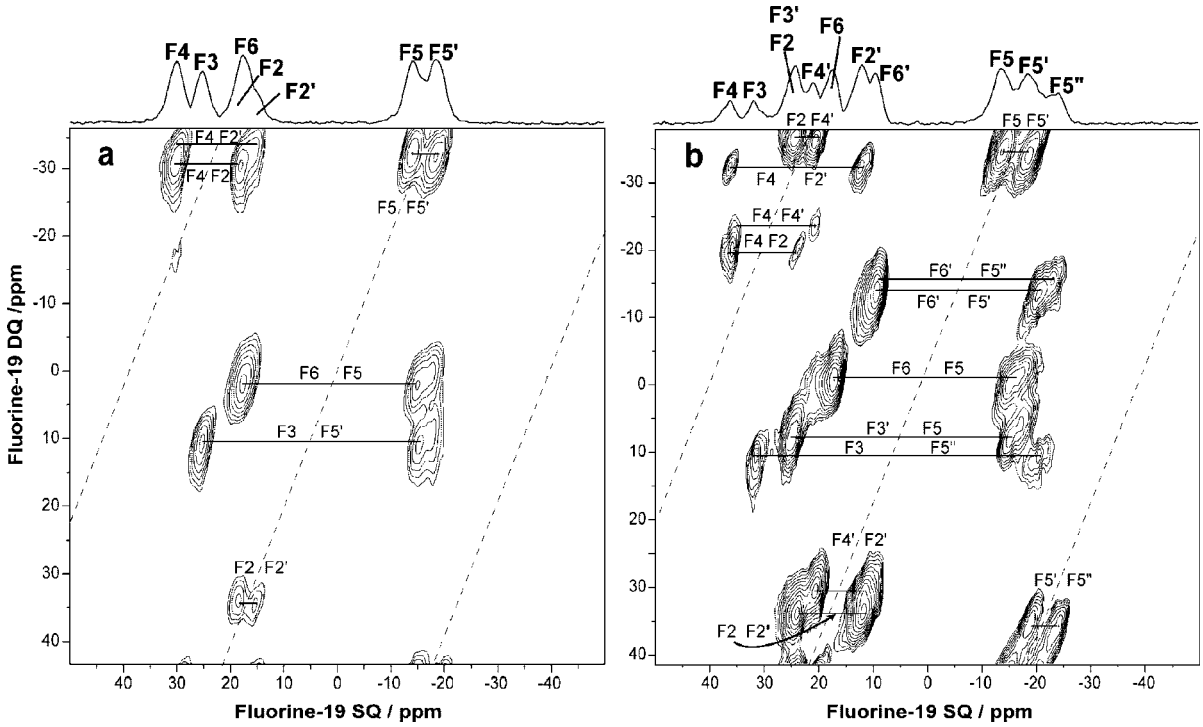

Figure 6. 2D DQ ^{19}F MAS NMR correlation spectra of TAF16-PYR collected at a sample temperature of (a) 327 and (b) 253 K with $\nu_R = 30$ kHz using a 66.6 μs excitation/reconversion BABA recoupling sequence. The single quantum projections are shown at the top.

Table 4. Selected F−F Distances in the Tantalum Oxyfluoride Clusters

compd	site–site	distance (Å)	$D_{ij}/2\pi$ (kHz)
	Intramolecular		
TAF24-IMI	F3−F5	2.64	5.87
	F6−F5	2.64	5.87
	F3−F6	2.62	6.01
	F4−F4	2.62	6.01
	F5−F4	3.49	2.54
	Intermolecular		
TAF24-IMI	F5−F4	3.24	3.18
	Intramolecular		
TAF24-TREN	F3−F5	2.41	7.72
	F6−F5	2.70	5.49
	F3−F6	2.65	5.81
	F4−F4	2.64	5.87
	F5−F4	3.23	3.21
	Intramolecular		
TAF16-PYR	F2−F2	2.64	5.87
	F4−F4	3.78	2.00
	F2−F4	2.62	6.01
	F5−F5	2.57	6.37
	F3−F6	3.76	2.03
	F5−F3	2.66	5.74
	F5−F6	2.67	5.68
	F3−F4	3.60	2.32
	Intermolecular		
TAF16-PYR	F3−F3	3.26	3.12
	F2−F5	3.14	3.49

the Ta(2) (F3, F5, and F6). Unfortunately, the F3, F5 and F6 sites can not be assigned uniquely from dipolar-based experiments since they equal distant to each other (Table 4). The subsequent spectral assignment of these sites was based on chemical shift trends and ab initio calculations as discussed in a later section. The similarity between the DQ MAS NMR spectra in Figures 5a and 5b demonstrates that the overall structure of the $[Ta_8F_{24}O_{12}]^{8-}$ cluster is similar for TAF24-IMI and TAF24-TREN, a fact used in the powder refinement of the TAF24-TREN structure. Finally, constraints on observable F−F contact distances in the DQ ^{19}F MAS NMR experiment can be estimated. Specifically, the F4 site shows no cross-correlations even though the F5 site has a 3.24 Å (intermolecular) and a 3.49 Å (intramolecular) contact with the F4 site. Therefore, F−F contact distances greater than 3.24 Å should not be observed in the DQ MAS of the TAF16-PYR.

The 2D DQ MAS NMR spectra for TAF16-PYR collected at a sample temperature of 327 and 253 K are shown in Figure 6. These spectra are more complicated with numerous correlation peaks being observed. These DQ NMR spectra allow the identification of resonances that were significantly overlapped in the 1D ^{19}F MAS NMR spectrum. Again the autocorrelation condition in the DQ spectra is denoted by the diagonal dashed lines. For this TAF16 cluster no autocorrelation peaks are observed at either temperature clearly showing that each of the different ^{19}F resonances results from single fluorine nuclei spatially removed from fluorines in similar environments. In the ^{19}F MAS NMR the F5 and F2 environments are inequivalent at both 327 and 253 K (and are denoted as 2, 2′ and 5, 5′). These NMR inequivalent fluorine environments show cross-correlations to each other (see Figure 6a) demonstrating that the 2 and 2′ or the 5 and 5′ fluorines are spatially near each other, and most likely bonded to the same tantalum. At lower temperatures, multiple resonances are observed for each of the other fluorine environment. This experimental observation is consistent with the multiple inequivalent chemical shifts obtained from ab initio calculations of proposed structural motifs discussed in later sections.

^{19}F NMR Chemical Shift Assignments for TAF24. On the basis of the strong autocorrelation peak in the 2D DQ

^{19}F MAS NMR spectra the $\delta = -31.8$ (TAF24-IMI) and $\delta = -22.8$ (TAF24-TREN) peaks were assigned to the three equivalent fluorine sites (F4) located on Ta1 within the TAF24 cage structure (Figure 1). These F4 resonances did not show any DQ cross-correlation peaks (panels a and b in Figure 5) to any other ^{19}F resonances, consistent with the long (>3 Å) intra and intermolecular ^{19}F−^{19}F distances within the proposed XRD structure (Table 4). These long-range correlations were not observed even for 2D DQ experiments with twice the excitation/reconversion periods supporting the assignment as the isolated F4 environment.

The remaining ^{19}F NMR resonances in the TAF24 compounds all reveal cross-correlation peaks in the 2D DQ MAS correlation spectra (panels a and b in Figure 5) and are assigned to the F3, F5 and F6 sites. These fluorines are all equally distant from each other (Table 4) and are not easily distinguished by these DQ experiments. In addition, a series of ^{19}F{^{1}H} REDOR NMR experiments were performed on the TAF24-IMI and TAF24-TREN materials (see Figures S6−S9 and the REDOR section in the Supporting Information). Unfortunately the REDOR constraints obtained did not aid in the final ^{19}F NMR spectral assignment.

Results from solution NMR suggest that longer d^0-metal fluoride bonds give rise to more shielded (smaller δ) ^{19}F chemical shifts,[45] while studies of TaF_5 complexes suggest that the chemical shift trends depend on the ability of the bonding between tantalum and the ligand to employ the *d* orbitals of tantalum.[53] Using the Ta-F bond distance relationship the F5, F3, and F6 sites of the TAF24 cluster can be assigned to the $\delta = +10.4$, -8.3, and -39.3 resonances for TAF24-IMI, and to the $\delta = +7.1$, $+1.7$, and -44.6 resonances for TAF24-TREN, respectively (see Table 1 for Ta−F distances). The correlation plot between the ^{19}F NMR chemical shift and the Ta−F bond distance for the three materials is shown in Figure S10 (Supporting Information). Although the relationship holds well for the TAF24-IMI ($r^2 = 0.956$) and TAF16-PYR ($r^2 = 0.933$) compounds, the fit is much poorer for the TAF24-TREN material ($r^2 = 0.521$). In particular, the correlation plot would predict a significantly longer Ta-F(6) bond length (~1.97 Å) in TAF24-TREN than the 1.915 Å experimentally refined, based on the −44.6 ppm chemical shift observed for the F6 site. However, it should be noted that the bond distances for the TAF24-TREN structure were refined using soft distance constraints, and may have produced nonoptimal structure. There does not seem to be a universal correlation for these TAF compounds despite their similar structures with the slopes of the bond distance/chemical shift correlations varying between −982 and −439 ppm/Å for the TAF24-IMI and TAF24-TREN materials, a ~45% difference (see Figure S10 in the Supporting Information). The validity of this simple correlation model is further question by the assignments experimentally determined from the 2D DQ MAS data. In particular the chemical shift of −22.8 ppm in TAF24-TREN would be undoubtedly assigned to the F6 site by the chemical shift/bond-distance relationship and would improve the correlation coefficient (r^2) from 0.52 to 0.86. However, this

Table 5. Ab Initio ^{19}F NMR Chemical Shielding and Shifts for the TAF24 Clusters[a]

site	σ[gas][b] (ppm)	σ[cont][c] (ppm)	$\Delta\sigma$[d]	δ[gas][e] (ppm)	δ[cont][e] (ppm)
		TAF24-IMI			
F3	197 (1)[f]	189 (1)[f]	+8	−52	−42
F4	215 (2)[f]	215 (2)[f]	0	−70	−68
F5	187 (2)[f]	182 (2)[f]	+5	−42	−35
F6	212 (3)[f]	208 (3)[f]	+4	−67	−61
		TAF24-TREN			
F3	190 (0.6)[f]	183 (0.6)[f]	+7	−45	−36
F4	241 (0.1)[f]	242 (0.1)[f]	−1	−96	−95
	248 (0.1)[f]	249 (0.1)[f]	−1	−103	−102
F5	187 (0.5)[f]	183 (0.6)[f]	+4	−42	−36
F6	196 (0.8)[f]	191 (0.4)[f]	+5	−51	−44

[a] Calculations using B3LYP, TZVP for F and O, LANL2DZ ECP for Ta. [b] Calculation using isolated cluster in gas phase. [c] Calculation using cluster embedded in polarizable continuum model (PCM). See Experimental Section for additional details. [d] $\Delta\sigma = \sigma(\text{gas}) - \sigma(\text{cont})$. [e] $\delta = \sigma(\text{ref}) - \sigma(\text{sample})$, where $CFCl_3$ is the reference ($\sigma = +145$ ppm [gas] and +147 ppm [cont]). [f] Average and standard deviation of the theoretical calculations over the 6 fluorines for each of these environments.

^{19}F shift is uniquely assigned to the F4 sited on the basis of the autocorrelation resonance in the DQ MAS NMR spectra.

Ab initio calculations have been shown to accurately calculate ^{19}F NMR chemical shifts in many other systems including compounds with metal atoms.[54,55] Therefore, chemical shifts calculated using density functional theory (DFT) were used to assist in the assignment of the ^{19}F NMR. The ^{19}F shielding values and chemical shifts predicted for the TAF24-IMI and TAF24-TREN clusters are given in Table 5. Results for the isolated $[Ta_8F_{24}O_{12}]^{8-}$ cluster (extracted from the XRD structure) both in the gas phase and surrounded by a polarizable continuum are presented. Calculations with different dielectric constants for the polarizable continuum field did not significantly vary the calculated ^{19}F NMR shielding constants. The correlation plots between the experimental and theoretical chemical shifts for TAF24-IMI are shown in Figure 7a, These results confirm the assignment of the F6 and F4 environments, but still leave the absolute assignment of the F5 and F3 sites in question because they vary with the details of the calculation. Interestingly, the calculated F5 and F3 chemical shifts are highly influenced by the introduction of the polarizable continuum ($\Delta\sigma$, see Table 5), suggesting that the shielding of these fluorines may be influenced by the counter organic cation. We will tentatively retain the assignment of the F5 environment to the largest observed ^{19}F NMR chemical shift.

The correlation for the TAF24-TREN compound is significantly worse (Figure S11, Supporting Information) with for both the gas phase and continuum model. The ab initio calculation also predicts the F4 chemical shift being −40 ppm smaller and the F6 chemical shift +40 ppm from the generalized linear correlation. This would suggest that the Ta-F6 bond distance should be increased, whereas the Ta−F4 bond distance decreased. These results clearly point to inaccuracies of the Ta−F bond lengths for the TAF24-TREN structure, and most likely arise from the use of soft

(53) Sala-Pala, J.; Calves, J. Y.; Guerchais, J. E.; Brownstein, S.; Dewan, J. C.; Edwards, A. J. *Can. J. Chem.* **1978**, 56.

(54) Schreckenbach, G. *Int. J. Quantum Chem.* **2005**, *101*, 372.

(55) Body, M.; Silly, G.; Legein, C.; Buzaré, J.-Y. *J. Phys. Chem. B* **2005**, *109*, 10270.

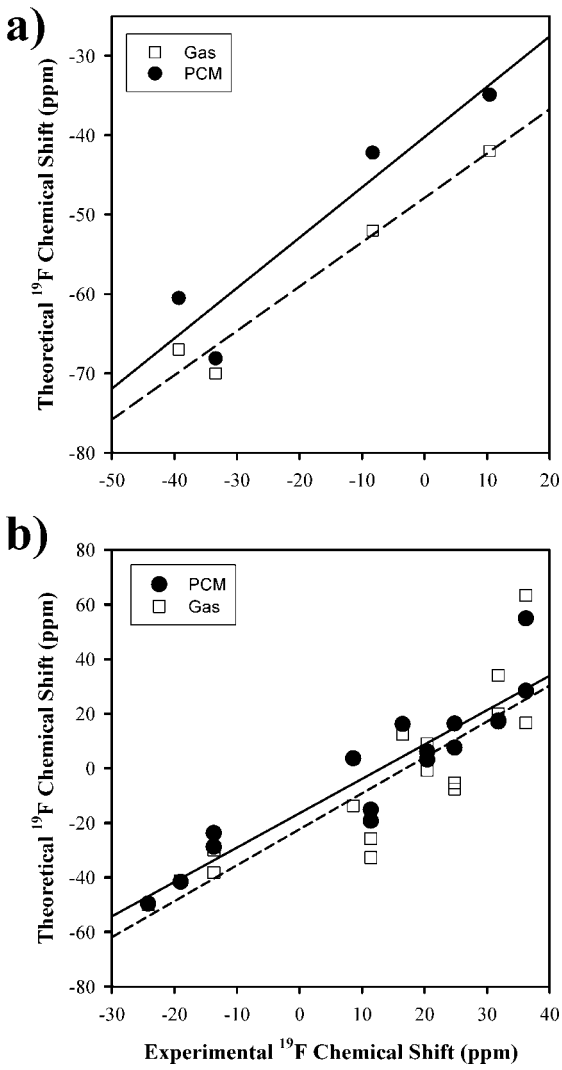

Figure 7. Correlation between experimental and ab initio ^{19}F NMR chemical shifts for the (a) TAF24-IMI cluster and (b) the TAF16-PYR cluster using a gas phase and a continuum model. The correlations were fit to $\delta^{theory} = a\delta^{exp} + b$, with $a = 0.56$, $b = -47.9$, and $r^2 = 0.96$ (TAF24-IMI, gas), $a = 0.63$, $b = -40.2$, and $r^2 = 0.89$ (TAF24-IMI, PCM), $a = 1.31$, $b = -22.3$, and $r^2 = 0.74$ (TAF16-PYR, gas), and $a = 1.26$, $b = -16.5$, and $r^2 = 0.85$ (TAF16-PYR, PCM)

constraints in the structure refinement of the powder XRD. The present TAF24-TREN structure should be considered a low-resolution result, and awaits further structural refinement.

^{19}F NMR Chemical Shift Assignments for TAF16. The assignment of the TAF16-PYR ^{19}F NMR spectra is slightly more complicated because there is not a unique autocorrelation resonance (like the F4 environment in the TAF24 materials) observed in the DQ ^{19}F MAS NMR spectra. Still, the dipolar coupling patterns observed in the DQ experiments are important for the assignment of the different ^{19}F NMR resonances. On the basis of the F−F distances reported from the XRD structure (Table 4), and the range of dipolar couplings probed in the DQ MAS NMR experiment, cross-correlation resonances should be observed between the F2/F4 environments and between the F3/F5 and F5/F6 environments, but no correlation between the F3/F6 or F4/F4 sites. The Ta1-F5 is the longest Ta-F bond in the cluster and is assigned to the resonances at $\delta = -14.2$ (F5) and -17.7 (F5′) (327 K, Figure 6a). The ab initio chemical shift calculations based on both the 300 K and the 168 K structures for TAF16-PYR are summarized in Table 6. While there are 16 different F within the cluster their chemical shifts can be group based on the F position within the cluster. For equivalent positions (at 300 K) the calculated chemical shifts typically vary by less that 0.5 ppm, while the experimental line widths are on the order of ∼3 ppm. The exception to this is the predicted chemical shifts of the F5 environments which group into 2 subsets separated by ∼2 ppm, and are designated as F5 and F5′, consistent with the F5 and F5′ resonances observed experimentally. The inequivalent F2 and F2′ environments observed experimentally differ from the ab initio calculations which predicted only a 0.5 ppm differences between F environments (Table 6). The observation of F5/F5′ and F2/F2′ DQ cross peaks shows that these nonequivalent fluorines are spatially near each other, are attached to the same Ta, and do not arise from a variation in local environments between different clusters or different domains within the material.

Assignment of the F5 and F5′ resonances provide the starting point for the subsequent ^{19}F NMR assignments of TAF16-PYR. The DQ NMR shows dipolar connectivity between the F5/F5′ sites (see Figure 6a) and $\delta = +18.0$ and $+25.4$, which are assigned to F6 and F3, respectively. The relative assignment of the F3 and F6 resonances was based on the ab initio calculations which predicted that the F3 environment had a 7 ppm larger chemical shift (smaller shielding) than the F6 fluorine environment. Unfortunately, there does not appear to be any clear way to experimentally distinguish these two fluorine sites. The other DQ dipolar network is observed via cross peaks between $\delta = +18.0$ and $+30.1$, and has been assigned to the F2/F2′ and F4 environments, respectively. These assignments are consistent with both the Ta-F bond length arguments and the ab initio results (Table 6). It should be noted that for TAF16-PYR there is considerable overlap between the F4/F3/F6/F2/F2′ ^{19}F NMR resonances, such that reordering of the resonance assignments would improve the correlation between predicted and experimental chemical shifts. The unique dipolar coupling patterns imposed by the DQ correlation experiments constrains this reordering in that peak assignment must also conform to the coupling patterns as discussed above. These DQ constraints also impact the ^{19}F assignments on the basis of simple Ta−F bond length arguments. For example, the correlation shown in Figure S10 (Supporting Information) would incorrectly inverse the F4 and F6 assignment, while the DQ correlation to the F5/F5′ environments ($\delta = -14.2/-17.7$, in Figure 6a) clearly defines the F6 site.

Both the variable-temperature (VT) ^{19}F MAS NMR and the low temperature 2D DQ ^{19}F MAS NMR correlation experiment reveal additional complex and dynamic behavior of the TAF16-PYR material. With decreasing temperature there is a splitting of all the resonances into multiple peaks. The low temperature crystal structure (168 K) shows an increase in oxygen disorder with decreasing temperature. Ab initio chemical shift calculations for the TAF16-PYR cluster incorporating one disordered oxygen site (out of four possible

Table 6. Ab initio ^{19}F NMR Chemical Shielding and Shifts for TAF16-PYR[e]

300 K structure[a]						168 K structure[a]					
site	σ[gas][a] (ppm)	σ[cont][b] (ppm)	δ[gas][a,c] (ppm)	δ[cont][b,c] (ppm)	δ[exp][c,d] (ppm)	site	σ[gas][a] (ppm)	σ[cont][b] (ppm)	δ[gas][a,c] (ppm)	δ[cont][b,c] (ppm)	δ[exp][c,e] (ppm)
F2	165.1	152.1	−20.1	−5.1	+18.0	F2	150.3	130.6	−5.3	+16.4	+24.8
	165.9	153.1	−20.9	−6.1			152.6	139.4	−7.6	+7.6	
F2′	166.5	154.7	−21.5	−7.7	+14.8	F2′	170.7	162.2	−25.7	−15.2	+11.4
	166.5	154.1	−21.5	−7.1			177.7	166.2	−32.7	−19.2	
F3	156.3	155.0	−11.3	−9.3	+25.4	F3	111.0	129.4	+15.6	+17.6	+31.8
	156.3	154.9	−11.3	−7.9		F3′	125.1	129.9	+19.9	+17.1	+24.8
F4	130.2	131.2	+14.8	+15.8	+30.1	F4	81.5	92.1	+63.5	+54.9	+36.2
	131.0	130.8	+13.9	+16.2			128.4	118.6	+16.6	+28.4	+20.4
	129.9	130.5	+13.9	+16.5		F4′	136.0	140.9	+9.0	+6.1	
	130.7	131.2	+14.3	+15.8			145.7	143.8	−0.7	+3.2	
F5	182.3	179.7	−37.3	−32.7	−14.2	F5	174.9	170.7	−25.7	−23.7	−13.7
	182.6	179.5	−37.6	−32.5	−14.2		183.2	175.7	−38.2	−28.7	−19.0
F5′	180.4	177.3	−35.4	−30.3	−17.7	F5′	186.2	188.6	−41.2	−41.6	−19.0
	180.4	176.9	−35.4	−29.9		F5″	195.5	196.6	−50.5	−49.6	−24.2
F6	135.1	143.9	+9.9	+3.1	+8.0	F6	132.6	130.8	+12.4	+16.2	+16.5
	135.4	144.6	+9.6	+2.4		F6′	158.7	150.7	−13.7	−3.7	+8.6

[a] Calculation based on refined 300 or 168 K structure (with 1 disordered oxygen). [b] Calculation using isolated cluster in vacuum (gas) or embedded in polarizable continuum model (PCM). [c] $\delta = \sigma$(ref) − σ(sample), where $CFCl_3$ is the reference, σ(gas) = 145 ppm and σ(cont) = 147 ppm. [d] Experimental ^{19}F chemical shifts at 327 K. [e] Experimental ^{19}F chemical shifts at 253 K.

oxygen sites) are presented in Table 6. On the basis of the ab initio calculations, the introduction of a disordered oxygen site can produce line splitting up to 30 ppm. For example, see the F2/F2′ and F4 calculated chemical shifts for the 168 K structure in Table 6. These large chemical shift changes occur because of the variation in the Ta−O−Ta bond angle, and without changes to either the Ta−F bond length or the F−Ta−F bond angle. This observation supports the argument that the observed VT behavior of TAF16-PYR is a result of increased oxygen disorder within the ring structure at lower temperatures. The linear correlation between the experimental (253 K) and the predicted ^{19}F NMR chemical shifts is shown in Figure 7b. Despite the reduced correlation in comparison to TAF24-IMI, the calculated-shift assignments of the different fluorine environments of TAF16-PYR (Table 3) are consistent with the DQ MAS experiment. It may be at even lower temperature these dynamics and changes in the ^{19}F chemical shifts would show increased agreement. Unfortunately, under high-speed MAS NMR conditions, we are not able to reach the 173 K used for the XRD analysis. It is also important to note that the slopes of the TAF24 and TAF16 chemical shift correlations (Figure 7) differ by approximately a factor of 2, precluding the direct use of these correlations in the analysis of ^{19}F NMR for unknown TAF clusters.

Oxygen−Fluorine Disorder. To address the impact of fluorine substitution for the bridging oxygens within the TAF clusters, we also performed a series of ab initio shielding calculations on the TAF16-PYR cluster, where the O1 or O2 oxygen environment was replaced by F. The ^{19}F NMR chemical shielding values are provided in Table S7 (Supporting Information). The substitution of a bridging O by a F atom removes the symmetry inherent within the cluster such that 16 distinct ^{19}F resonances are predicted for the TAF17 clusters (F-substituted TAF16 cluster). The experimental observation of only six distinct resonances in the TAF16-PYR material (327 K) argues against such substitution. In addition, the fluorine/oxygen substitution results in a general deshielding of the fluorine adjacent to the substitution site on the order of 60 ppm (increased chemical shift), whereas fluorines remote to the substitution site experienced only a ∼25 ppm deshielding (increase in the chemical shift). The impurity resonance at $\delta = -198.7$ was originally thought to be a disordered Ta−F−Ta environments within this material. These ab initio results argue against this by predicting Ta−F−Ta species to occur ∼25 ppm shielded (lower chemical shift) from the most shielded Ta−F environment. This would predict a Ta−F−Ta resonance between approximately $\delta = -50$ and -75. This prediction is close to the $\delta(^{19}F) = -58.5$ reported for bridging fluorines in $TaCl_2F_3$ melts[56] or the −80.8 reported for a bridging fluoride within the $[Ta_2F_{11}]^-$ species in solution.[57] There are no ^{19}F NMR resonances observed experimentally in this region for the TAF16 or TAF24 materials, again providing further evidence that fluorine exchange for oxygen and the resulting disorder are not present within these TAF materials. In addition, the $\delta = -198.7$ resonance does not correspond to the ^{19}F NMR chemical shifts reported for the TaF_6^- anion which was reported at −40 ppm.[56,58] The identity of this small impurity resonance has not been determined. These F/O exchange calculations also support our refinement of the oxygen disorder as resulting purely from fractional occupation and not fluorine−oxygen substitutional disorder.

Impact of Computational Model on the ^{19}F Chemical Shift. The assignments and discussion presented above were based in part on hybrid-DFT calculations in the Gaussian program. The presence of the Ta atoms within the cluster may give rise to "heavy-atom effects" on the NMR shielding of the bonded ^{19}F nuclei. The impact of scalar relativistic and spin–orbit effects of the heavy atom Ta were not explicitly included in those DFT calculations, and thus the relativistic effects were evaluated using the ZORA method as implemented by ADF. The ^{19}F NMR chemical shielding and chemical shifts for the TAF16-PYR cluster (168 K structure) using these different models are summarized in Tables S8 and S9 (Supporting Information), with the predicted and experimental chemical shift correlation

(56) Buslaev, Y. A.; Ilyin, E. G. *J. Fluorine Chem.* **1974**, *4*, 271.
(57) Brownstein, S.; Latermouille, G. *Can. J. Chem.* **1974**, *52*, 2236.
(58) Buslayev, Y. A.; Kokunov, Y. V.; Kopanev, V. D.; Gustyakova, M. P. *J. Inorg. Nucl. Chem.* **1974**, *36*, 1569.

shown in Figure S12 (Supporting Information). The relativistic models show considerable *y*-intercepts and are most likely due to the influence of the crystal environment in the solid-state NMR measurements, which were not explicitly treated in the cluster model computations. It should be noted that recent ab initio investigations of uranium fluoride chlorides have suggested that the approximate exchange correlation functional may also be a source of errors.[54] Overall, the ^{19}F NMR chemical shift range is reasonably well reproduced by the computations and the trends are consistent between the different computational models as seen in the similar correlation slopes. We did not find a significant improvement by performing the much more expensive ZSO (including spin–orbit coupling) computations over the ZSC (spin-free relativistic computations). Interestingly, the non-relativistic (NR) ADF results are quite close to the G03/B3LYP results, which were obtained with the scalar relativistic ECP, LANL2DZ, for the Ta atoms. These results suggest that a hybrid density functional may improve the ZSC and ZSO computations. Therefore, we have feel these trends justify using the G03/B3LYP(LANLDZ) results for the computation-based assignment of the ^{19}F NMR chemical shifts of the $[Ta_4F_{16}O_4]^{4-}$ and $[Ta_8F_{24}O_{12}]^{8-}$ anion clusters (as described above).

Conclusions

The structures of three novel tantalum oxyfluoride compounds have been studied by XRD and SSNMR. Methods for assigning the ^{19}F NMR chemical shifts to these unique structures have been discussed. These methods include the 2D DQ ^{19}F MAS NMR correlation experiment, correlation between Ta−F bond distance and ^{19}F chemical shifts, and ab initio calculated chemical shifts. The SSNMR results showed significant dynamics and inequivalent nature of the fluorine atoms. Variable temperature studies reveal that the smaller ringlike $[Ta_4F_{16}O_4]^{4-}$ cluster is significantly more dynamic with increased oxygen disorder than the cage-like structure of the $[Ta_8F_{24}O_{12}]^{8-}$ cluster. Linear correlations between the experimental and predicted ^{19}F NMR chemical shifts for the TAF24-IMI and TAF16-PYR structures are observed. Deviations between experimental and predicted ^{19}F chemical shifts in the TAF24-TREN structure suggest further refinement of this powder based structure is warranted. The influence of relativistic affects on the ab initio ^{19}F chemical shift calculations was also demonstrated to have a minimal impact.

Acknowledgment. Sandia is a multiprogram laboratory operated by Sandia Corporation, a Lockheed Martin Company, of the United States Department of Energy's National Nuclear Security Administration under Contract DE-AC04-94AL85000. This work was supported by the U.S. Department of Energy BES program.

Supporting Information Available: Crystallographic information in CIF format; ^{19}F MAS NMR under different decoupling conditions and a different magnetic field strength, VT ^{13}C MAS NMR, ^{19}F shielding versus Ta−F bond distance correlations, ^{19}F{^{1}H} REDOR results and simulations, SEM of TAF16-PYR, along with tables and figures containing ab initio ^{19}F NMR shielding calculations, tables containing structural refinement details, and tables of bond valence sums (PDF). This material is available free of charge via the Internet at http://pubs.acs.org.

CM0717763